

Intra-unit-cell electronic nematicity of the high- T_c copper-oxide pseudogap states

M. J. Lawler^{1,2*}, K. Fujita^{2,3,4*}, Jhinwan Lee^{2,3,5}, A. R. Schmidt^{2,3}, Y. Kohsaka⁶, Chung Koo Kim^{2,3}, H. Eisaki⁷, S. Uchida⁴, J. C. Davis^{2,3,8}, J. P. Sethna² & Eun-Ah Kim²

In the high-transition-temperature (high- T_c) superconductors the pseudogap phase becomes predominant when the density of doped holes is reduced¹. Within this phase it has been unclear which electronic symmetries (if any) are broken, what the identity of any associated order parameter might be, and which microscopic electronic degrees of freedom are active. Here we report the determination of a quantitative order parameter representing intra-unit-cell nematicity: the breaking of rotational symmetry by the electronic structure within each CuO_2 unit cell. We analyse spectroscopic-imaging scanning tunnelling microscope images of the intra-unit-cell states in underdoped $\text{Bi}_2\text{Sr}_2\text{CaCu}_2\text{O}_{8+\delta}$ and, using two independent evaluation techniques, find evidence for electronic nematicity of the states close to the pseudogap energy. Moreover, we demonstrate directly that these phenomena arise from electronic differences at the two oxygen sites within each unit cell. If the characteristics of the pseudogap seen here and by other techniques all have the same microscopic origin, this phase involves weak magnetic states at the O sites that break 90° -rotational symmetry within every CuO_2 unit cell.

The pseudogap phase emerges in the CuO_2 plane (Fig. 1a) upon removal of electrons from the O atoms of the parent ‘charge-transfer’² Mott insulator (Fig. 1b). At low hole-density p , two fundamentally distinct types of electronic excitations are observed³ (Fig. 1c). Here the lower-energy branch of excitations Δ_0 appears to be associated with the maximum energy of Cooper pairing⁴. The higher-energy branch labelled Δ_1 is the spectroscopic ‘pseudogap’ because the same energy gap exists in both the superconducting and pseudogap phases (Fig. 1b). Moreover, Δ_1 tracks T^* , the temperature at which pseudogap phenomenology appears, as a function of doping, implying that Δ_1 is the energy gap associated with any electronic symmetry breaking at T^* . Therefore the question of which symmetries are broken at T^* is equivalent to that of which broken symmetries the excitations with energy Δ_1 exhibit.

The ‘pseudogap states’ at energy $\omega \approx \pm \Delta_1$ can be examined directly using tunnelling spectroscopy. Figure 1d shows the evolution of spatially averaged conductance spectra⁴ with the doping dependence of $\pm \Delta_1$ indicated by blue dashed curves. Figure 2a and b shows atomically resolved electronic structure images with $\omega \approx \Delta_1$ (refs 5 and 6) acquired at $T < T_c$ (Fig. 2a) and $T > T_c$ (Fig. 2b) for an underdoped $\text{Bi}_2\text{Sr}_2\text{CaCu}_2\text{O}_{8+\delta}$ sample with $T_c \approx 35$ K. The insets show that their Fourier transforms are dominated by four inequivalent non-dispersive wavevectors labelled \mathbf{Q}_x , \mathbf{Q}_y , \mathbf{S}_x and \mathbf{S}_y . These phenomena are indistinguishable above and below T_c (refs 5 and 6 and Fig. 2), so the spatial symmetries of the pseudogap states can be established to the highest precision by using the $T \approx 0$ experiments. A striking feature of

such pseudogap state images in $\text{Bi}_2\text{Sr}_2\text{CaCu}_2\text{O}_{8+\delta}$ (refs 5–8) and $\text{Ca}_{2-x}\text{Na}_x\text{CuO}_2\text{Cl}_2$ (ref. 5) is the apparent local breaking of 90° rotation (C_4) symmetry at the unit-cell scale. Lattice-translation symmetry is also broken locally at the nanoscale, yielding broad peaks around \mathbf{S}_x and \mathbf{S}_y (refs 5 and 6). Theoretical analyses of such images have posited disordered smectic electronic liquid crystals or stripes^{9,10}.

Indeed, from the perspective of symmetry, the spatial arrangements of the pseudogap states^{5–8} exhibit similarities to those of liquid crystals. Electronic liquid crystals have been defined^{11–17} to arise when the electronic structure breaks spatial symmetries of the crystal lattice (any resultant lattice symmetry changes may or may not be detectable¹⁶). Nematic phases preserve the (lattice) translational symmetry and break the rotational (point group) symmetry, whereas smectic and striped phases break both^{10–17}. Correlated electronic systems exhibiting evidence for electronic nematicity include $\text{Sr}_3\text{Ru}_2\text{O}_7$ (ref. 18) and $\text{CaFe}_{1.94}\text{Co}_{0.06}\text{As}_2$ (ref. 19). Microscopic models for both systems posit nematicity due to a C_4 symmetry breaking which renders the d_{xz} and d_{yz} orbitals of each Ru or Fe atom inequivalent^{20–23}. For copper oxides, the local 180° rotational (C_2) symmetry observed in the pseudogap states^{5,6,8} implied the possibility of electronic nematicity but with contributions from multiple sites within the CuO_2 cell (shown schematically in Fig. 2c).

Here we focus on C_4 to C_2 symmetry reduction in sub-unit-cell resolution images of the copper-oxide pseudogap states^{5,6,8}. We introduce a general measure of electronic nematicity in any image $M(\mathbf{r})$:

$$O_n[M] = \frac{1}{2} [\tilde{M}(\mathbf{Q}_y) - \tilde{M}(\mathbf{Q}_x) + \tilde{M}(-\mathbf{Q}_y) - \tilde{M}(-\mathbf{Q}_x)] \quad (1)$$

$$= \text{Re}\tilde{M}(\mathbf{Q}_y) - \text{Re}\tilde{M}(\mathbf{Q}_x)$$

Here $\tilde{M}(\mathbf{q}) = \text{Re}\tilde{M}(\mathbf{q}) + i\text{Im}\tilde{M}(\mathbf{q})$, the complex-valued two-dimensional Fourier transform of any $M(\mathbf{r})$ with its origin at a Cu site, is evaluated at inequivalent Bragg peaks $\mathbf{Q}_x = (2\pi/a_0)\mathbf{x}$ and $\mathbf{Q}_y = (2\pi/a_0)\mathbf{y}$, and a_0 is the unit-cell dimension. Figure 1a illustrates why only $\text{Re}\tilde{M}(\mathbf{Q})$ enters the definition of $O_n[M]$ by showing it in phase with the Cu lattice (even about each Cu site). By focusing on the Bragg peaks, $O_n[M]$ locks onto only those electronic phenomena with the same spatial periodicity as the crystal and then quantifies the C_4 symmetry breaking. Importantly, this generic order parameter in equation (1) will be widely applicable to data from other techniques. Successful application of equation (1) for spectroscopic-imaging scanning tunnelling microscopy (STS) images requires (1) a highly accurate registry of each Cu site location in $M(\mathbf{r})$ to satisfy the extreme sensitivity of $O_n[M]$ to the phase of $\tilde{M}(\mathbf{Q}_{x,y})$, and (2) that $M(\mathbf{r})$ has the sub-unit-cell

¹Department of Physics, Applied Physics and Astronomy, Binghamton University, Binghamton, New York 13902-6000, USA. ²Laboratory for Atomic and Solid State Physics, Department of Physics, Cornell University, Ithaca, New York 14853, USA. ³Condensed Matter Physics and Materials Science Department, Brookhaven National Laboratory, Upton, New York 11973, USA. ⁴Department of Physics, University of Tokyo, Bunkyo-ku, Tokyo 113-0033, Japan. ⁵Department of Physics, Korea Advanced Institute of Science and Technology, 373-1 Guseong-dong, Yuseong-gu, Daejeon 305-701, Korea. ⁶Magnetic Materials Laboratory, RIKEN, Wako, Saitama 351-0198, Japan. ⁷Institute of Advanced Industrial Science and Technology, Tsukuba, Ibaraki 305-8568, Japan. ⁸School of Physics and Astronomy, University of St. Andrews, North Haugh, St Andrews, Fife KY16 9SS, Scotland.

*These authors contributed equally to this work.

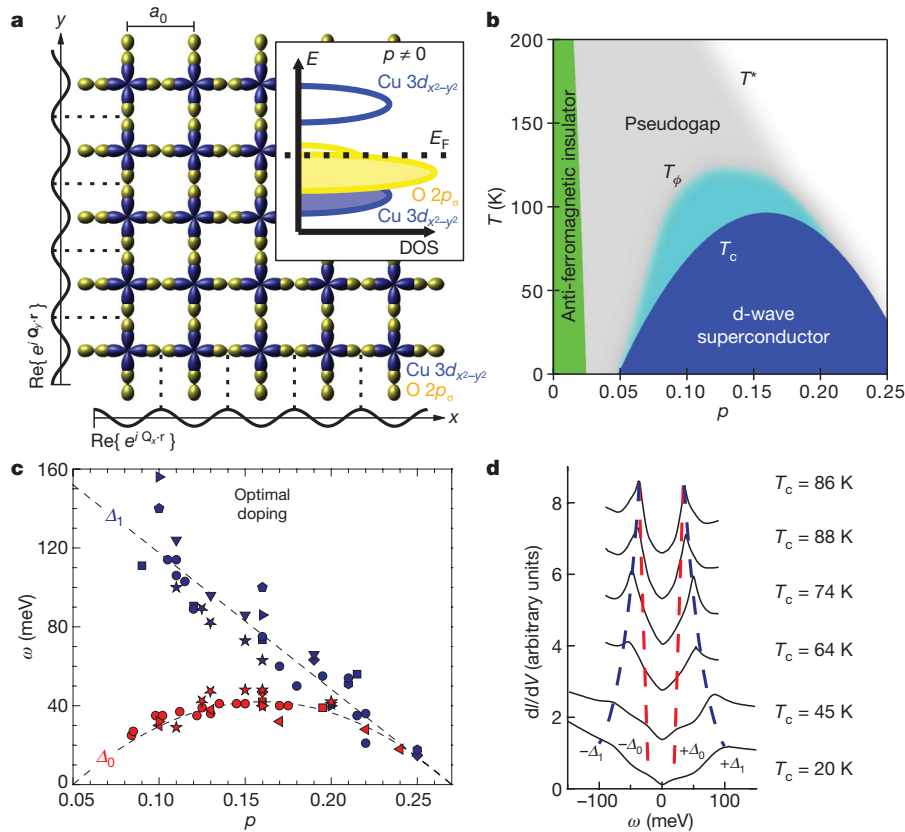


Figure 1 | CuO₂ electronic structure and $\omega \approx \Delta_1$ pseudogap states.

a, Schematic of the spatial arrangements of CuO₂ electronic structure with Cu sites and $d_{x^2-y^2}$ orbitals indicated in blue and O sites and $2p_z$ orbitals in yellow. E_F , Fermi energy. The inset shows the approximate energetics of the band structure when such a charge-transfer insulator is doped by removing electrons from the O atoms (the respective bands are indicated by the same colours as in the CuO₂ schematic). The ‘real’ part of any \mathbf{q} -space electronic structure at the Bragg wavevector $\text{Re}\tilde{M}(\mathbf{Q}, \omega)$ is defined throughout this paper as being in phase with the Cu lattice (and therefore even about each Cu site). This definition is shown schematically as modulations in $\tilde{M}(\mathbf{r}, \omega)$ which would contribute to $\text{Re}\tilde{M}(\mathbf{Q}, \omega)$ at the two Bragg wavevectors \mathbf{Q}_x and \mathbf{Q}_y . DOS, density of states. **b**, Schematic copper-oxide phase diagram. Here T_c is the critical temperature circumscribing a ‘dome’ of superconductivity, T_ϕ is the maximum temperature at which phase fluctuations are detectable

resolution without which $O_n[M]$ will be identically zero. $O_n[M]$ would also be identically zero if only the Cu sites $\mathbf{R} = (ma_0, na_0)$ (with m, n integers) contribute to $M(\mathbf{r})$ because then $\tilde{M}(\mathbf{Q}_x) \equiv \tilde{M}(\mathbf{Q}_y)$. In contrast, if all three atomic sites within each CuO₂ unit cell contribute to $M(\mathbf{r})$, then:

$$\begin{aligned}\tilde{M}(\mathbf{Q}_x) &= \bar{M}_{\text{Cu}} - \bar{M}_{\text{O}_x} + \bar{M}_{\text{O}_y} \\ \tilde{M}(\mathbf{Q}_y) &= \bar{M}_{\text{Cu}} + \bar{M}_{\text{O}_x} - \bar{M}_{\text{O}_y} \\ O_n[M] &= 2(\bar{M}_{\text{O}_x} - \bar{M}_{\text{O}_y})\end{aligned}\quad (2)$$

where \bar{M}_{Cu} , \bar{M}_{O_x} and \bar{M}_{O_y} are the average of $M(\mathbf{r})$ at the Cu, O_x and O_y sites respectively. The last line follows from equation (1). Hence detection of $O_n[M] \neq 0$ would imply that an inequivalence exists between the electronic structure at the O_x and O_y sites, as shown schematically in Fig. 2c.

Standard differential conductance mapping of $dI/dV(\mathbf{r}, \omega = eV) \equiv g(\mathbf{r}, \omega)$ to image the local density of states $N(\mathbf{r}, \omega)$ is challenging in strongly underdoped copper-oxides^{5–8} because of the intense electronic heterogeneity. However, imaging the ratio $Z(\mathbf{r}, \omega) \equiv \frac{g(\mathbf{r}, +\omega)}{g(\mathbf{r}, -\omega)} \equiv \frac{N(\mathbf{r}, +\omega)}{N(\mathbf{r}, -\omega)}$ avoids these severe systematic errors^{5–8} (Supplementary Information section I). Another challenge is the

within the pseudogap phase, and T^* is the approximate temperature at which the pseudogap phenomenology first appears. **c**, The two distinct classes of excitations as identified by multiple spectroscopies in underdoped copper-oxides (reproduced with permission from ref. 3) as a function of hole-density p . The excitations to energies $\Delta_1(p)$ are referred to as the ‘pseudogap states’ both because $\Delta_1(p)$ tracks $T^*(p)$ and because they exist unchanged in both the pseudogap and superconducting phases. Those excitations to energies $\omega < \Delta_0(p)$ can be associated with the Bogoliubov quasiparticles^{6–8}. **d**, Evolution of the spatially averaged tunnelling spectra of Bi₂Sr₂CaCu₂O_{8+δ} with diminishing p , here characterized by $T_c(p)$. The energies $\Delta_1(p)$ (blue dashed line) are easily detected as the pseudogap edge while the energies $\Delta_0(p)$ (red dashed line) are more subtle but can be identified by the correspondence of the ‘kink’ energy⁴ with the extinction energy of Bogoliubov quasiparticles, following the procedure in ref. 8.

random nanoscale variations of $\Delta_1(\mathbf{r})$; this problem can be mitigated⁸ by defining a reduced energy scale $e \equiv \omega/\Delta_1(\mathbf{r})$ which measures the energy at each position \mathbf{r} with respect to the pseudogap magnitude $\Delta_1(\mathbf{r})$ at that position, thus ensuring that the pseudogap states occur at $e \approx 1$ in all $Z(\mathbf{r}, e)$ data⁸. Using these techniques, a clearer picture of the two basic classes³ of electronic excitations in copper oxides has emerged^{5–8}. First, for all energies below $\omega \approx \Delta_0$ (a slowly doping-dependent energy⁸ indicated by the red dashed line in Fig. 1d) the electronic excitations are demonstrably^{5–8} Bogoliubov quasiparticles. Indeed, in both the superconducting^{5–8} and underdoped pseudogap⁶ phases, these dispersive low-energy states exhibit only the symmetries of a d -wave superconductor. The $\omega \approx \Delta_1$ pseudogap states are profoundly different, being non-dispersive^{5–8} and locally breaking crystal point-group symmetries. The challenge is therefore to identify first which symmetries are broken by the $\omega \approx \Delta_1$ pseudogap states and then the microscopic degrees of freedom involved in any such symmetry breaking.

We explore the intra-unit-cell electronic nematicity of Bi₂Sr₂CaCu₂O_{8+δ} by applying equation (1) to $\tilde{Z}(\mathbf{Q}_x, e)$ and $\tilde{Z}(\mathbf{Q}_y, e)$, the complex-valued two-dimensional Fourier transforms of $Z(\mathbf{r}, e)$ evaluated at \mathbf{Q}_x and \mathbf{Q}_y (red circles in Fig. 2). The sub-unit-cell resolution $Z(\mathbf{r}, e)$ imaging was performed on multiple different underdoped Bi₂Sr₂CaCu₂O_{8+δ} samples with values of T_c between

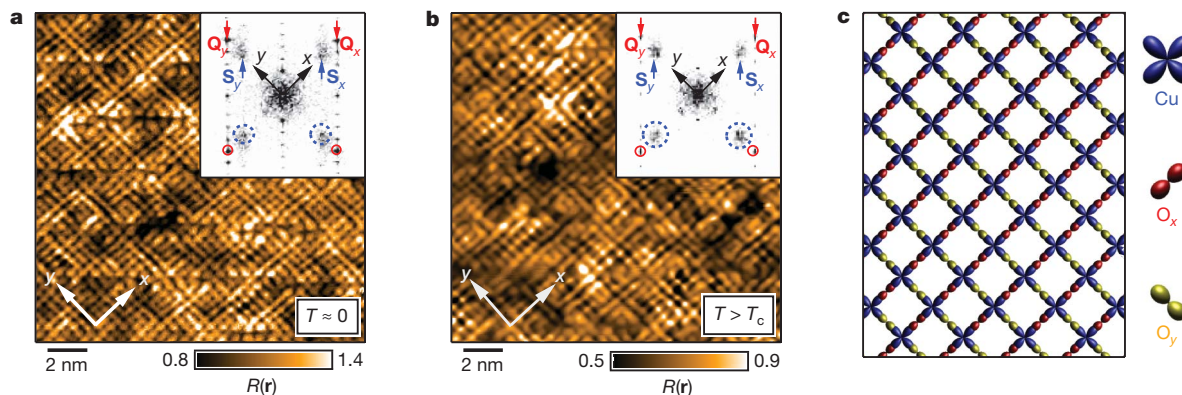


Figure 2 | Imaging the spatial symmetries of the $\omega \approx \Delta_1$ pseudogap states. **a**, Spatial image (R -map⁵) of the $\text{Bi}_2\text{Sr}_2\text{CaCu}_2\text{O}_{8+\delta}$ pseudogap states $\omega \approx \Delta_1$ at $T \approx 4.3$ K for an underdoped sample with $T_c = 35$ K. The inset shows the Fourier transform upon which the inequivalent Bragg vectors $\mathbf{Q}_x = (1, 0)2\pi/a_0$ and $\mathbf{Q}_y = (0, 1)2\pi/a_0$ are identified by red arrows and circles. The inequivalent wavevectors $\mathbf{S}_x = (\sim 3/4, 0)2\pi/a_0$ and $\mathbf{S}_y = (0, \sim 3/4)2\pi/a_0$ are identified by blue arrows and circles. **b**, Spatial image (R -map⁵) of the $\text{Bi}_2\text{Sr}_2\text{CaCu}_2\text{O}_{8+\delta}$ pseudogap states $\omega \approx \Delta_1$ at $T \approx 55$ K for the same sample with $T_c = 35$ K. Again, the inset shows the Fourier transform with the inequivalent Bragg

vectors $\mathbf{Q}_x = (1, 0)2\pi/a_0$ and $\mathbf{Q}_y = (0, 1)2\pi/a_0$ identified by red arrows and $\mathbf{S}_x = (\sim 3/4, 0)2\pi/a_0$ and $\mathbf{S}_y = (0, \sim 3/4)2\pi/a_0$ identified by blue arrows and circles. The phenomenology of the $\omega \approx \Delta_1$ pseudogap states, especially their broken spatial symmetries, appear indistinguishable whether in the superconducting phase (**a**) or in the pseudogap phase (**b**). **c**, A schematic representation of how electronic contributions from multiple sites within the CuO_2 unit cell could lead to global electronic nematicity in the copper oxides. Here the two O sites are labelled using different colours to represent the inequivalent electronic structure at those locations within each unit cell.

20 K and 55 K. The necessary registry of the Cu sites in each $Z(\mathbf{r}, e)$ is achieved by a picometre-scale realignment procedure that identifies a transformation to render the topographic image $T(\mathbf{r})$ perfectly a_0 -periodic (Supplementary Information section II). We then apply the same transformation to the simultaneously acquired $Z(\mathbf{r}, e)$ to register all the electronic structure data to this ideal lattice.

Such a topographic image $T(\mathbf{r})$ is shown in Fig. 3a; the location of every Cu site is known with a precision of about 10 picometres. The inset compares the Bragg peaks of its real (in phase) Fourier components $\text{Re}T(\mathbf{Q}_x)$ and $\text{Re}T(\mathbf{Q}_y)$ and demonstrates that $\text{Re}T(\mathbf{Q}_x)/\text{Re}T(\mathbf{Q}_y) = 1$. Therefore $T(\mathbf{r})$ preserves the C_4 symmetry of the crystal lattice. In contrast, Fig. 3b shows that $Z(\mathbf{r}, e = 1)$ determined simultaneously with Fig. 3a seems to break various crystal symmetries locally⁵⁻⁷. The inset showing that $\text{Re}\tilde{Z}(\mathbf{Q}_x, e = 1)/\text{Re}\tilde{Z}(\mathbf{Q}_y, e = 1) \neq 1$ reveals a remarkable discovery: the pseudogap states break C_4 symmetry throughout Fig. 3b. Therefore, following equation (1), we define a normalized order parameter over the entire field of view (FOV) for intra-unit-cell electronic nematicity as a function of e :

$$O_n^Q(e) \equiv \frac{\text{Re}\tilde{Z}(\mathbf{Q}_y, e) - \text{Re}\tilde{Z}(\mathbf{Q}_x, e)}{\tilde{Z}(e)} \quad (3)$$

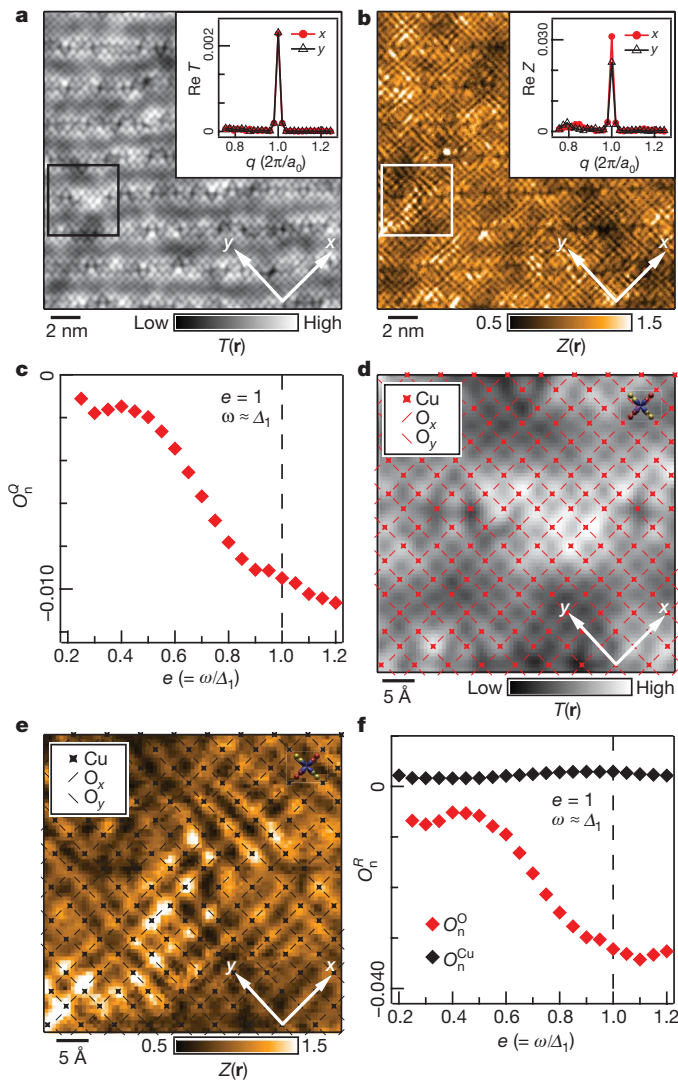
The plot of $O_n^Q(e)$ in Fig. 3c provides the second important discovery: the magnitude of $O_n^Q(e)$ is low for $e \ll 1$, only begins to grow near $e \approx \Delta_0/\Delta_1$, and becomes well defined near $e \approx 1$ ($\omega \approx \Delta_1 \approx 100$ meV in this sample). Hence, the electronic nematicity is associated with the pseudogap states. The low value of $|O_n^Q(e)|$ for small e is to be expected, because here the Bogoliubov quasiparticles are observed to respect the d -wave superconductor symmetries^{4,5,8}. The rapid increase in $|O_n^Q(e)|$ is primarily of electronic origin, because the normalization factor (the spatial average of $Z(\mathbf{r}, e)$) $\tilde{Z}(e) \approx 1$ for all e . Finally, equivalent $O_n^Q(e)$ analyses of all samples studied, measured using two different STMs, show results in agreement with Fig. 3 (Supplementary Information section III), with the exception that the opposite sign of $O_n^Q(e)$ can also be observed.

Equation (2) predicts that the predominant contributions to nematicity must come from the O sites (Fig. 2c). To test this idea directly, we examine $Z(\mathbf{r}, e)$ with sub-unit-cell resolution. Figure 3d shows the topographic image of a representative region from Fig. 3a; the locations of each Cu site \mathbf{R} and of the two O sites within its unit cell are indicated. Figure 3e shows $Z(\mathbf{r}, e)$ measured simultaneously with Fig. 3d with the same Cu and O site labels. To quantify the \mathbf{r} -space electronic nematicity we define the \mathbf{r} -space equivalent of equation (3):

$$O_n^R(e) = \sum_{\mathbf{R}} \frac{Z_x(\mathbf{R}, e) - Z_y(\mathbf{R}, e)}{\tilde{Z}(e)N} \quad (4)$$

Here $Z_x(\mathbf{R}, e)$ is the magnitude of $Z(\mathbf{r}, e)$ at the O site $a_0/2$ along the x -axis from \mathbf{R} while $Z_y(\mathbf{R}, e)$ is the equivalent along the y -axis, and N is the number of unit cells. Hence $O_n^R(e)$ counts only the O site contributions. Figure 3e shows the calculated value of $O_n^R(e)$ from the same FOV as Fig. 3a and b. It is obviously in good agreement with $O_n^Q(e)$, remaining at low amplitude for small e and then rapidly becoming established near the pseudogap states at $e \approx 1$. Thus, the electronic nematicity discovered using $O_n^Q(e)$ indeed derives primarily from the inequivalence of electronic structure at the two O sites within each unit cell. The energy dependence of the average unit-cell electronic structure (Supplementary Information section IV) shows directly that although electronic changes are undetectable at the Cu sites, they are observable at the O sites; this is an explicit demonstration that electronic nematicity in $O_n^Q(e)$ is associated with the O sites and the pseudogap energy. All these observations have been confirmed, using both independent measures $O_n^Q(e)$ and $O_n^R(e)$, in the other samples (Supplementary Information section III). Moreover, other possible sources of systematic error including tip-shape, STM head geometry, scan direction, and sub-atomic register of $Z(\mathbf{r}, e)$ to $T(\mathbf{r})$ have been ruled out positively for every tip/sample combination reported herein (Supplementary Information section V).

Evidence that a predominant symmetry of the pseudogap states of $\text{Bi}_2\text{Sr}_2\text{CaCu}_2\text{O}_{8+\delta}$ is that of an intra-unit-cell nematic motivates examination of any smectic characteristics in $Z(\mathbf{r}, e)$, because a smectic can melt into a nematic⁹⁻¹⁶. Originally the searches for smectic patterns focused on $g(\mathbf{r}, \omega)$ modulations with $\mathbf{Q}_{1/4,x} \approx (1/4, 0)2\pi/a_0$, $\mathbf{Q}_{1/4,y} \approx (0, 1/4)2\pi/a_0$ (refs 9, 10 and 12). However, all $\mathbf{Q}_{1/4,x}$ and $\mathbf{Q}_{1/4,y}$ features at low energy are actually dispersive Bogoliubov quasiparticle interferences⁶⁻⁸ and non-dispersive modulations with these \mathbf{Q} values become very weak in $Z(\mathbf{r}, e \approx 1)$ (Figs 2 and 3). Instead, the strong non-dispersive modulations at the pseudogap energy⁵⁻⁸ exhibit wavevectors $\mathbf{S}_x \equiv (\sim 3/4, 0)2\pi/a_0$, $\mathbf{S}_y \equiv (0, \sim 3/4)2\pi/a_0$ (blue circles in Fig. 2 insets) the magnitudes $|\mathbf{S}_x|$ and $|\mathbf{S}_y|$ of which are weakly doping-dependent⁸. There are two important points here: (1) our definition of intra-unit-cell nematicity using the Bragg peaks in equation (1) is independent of the \mathbf{S}_x , \mathbf{S}_y (or any other) smectic modulations and, (2) although \mathbf{S}_x and \mathbf{S}_y might seem related to $\mathbf{Q}_{1/4,x}$ and $\mathbf{Q}_{1/4,y}$ by reciprocal lattice vectors, the two sets of wavevectors are actually inequivalent in a $Z(\mathbf{q}, e)$ derived from a $Z(\mathbf{r}, e)$ resolving the three atomic sites within the unit cell.



To examine smectic spatial organization, we next define a measure analogous to equation (3) of C_4 symmetry breaking in modulations with S_x, S_y as:

$$O_s^Q(e) = \frac{\text{Re}\tilde{Z}(S_y, e) - \text{Re}\tilde{Z}(S_x, e)}{\tilde{Z}(e)} \quad (5)$$

For all samples studied, $|O_s^Q(e)|$ is found to be very low and independent of energy (Fig. 4b). Obviously, $|O_s^Q(e)|$ is low at low e because these states are dispersive Bogoliubov quasiparticles^{6–8} but, more importantly, $|O_s^Q(e)|$ shows no tendency to become well established at the pseudogap energy (Fig. 4b).

To separate the nematic and smectic contributions in $Z(\mathbf{r}, e)$, we examine the spatial fluctuations of each ordering tendency by defining coarse-grained \mathbf{r} -space order parameter fields $O_n^Q(\mathbf{r}, e)$ and $O_s^Q(\mathbf{r}, e)$ using the coarsening length scales $1/A_n$ and $1/A_s$ shown as red and blue circles in Fig. 2 (Supplementary Information section VI). The resulting $O_n^Q(\mathbf{r}, e)$ and $O_s^Q(\mathbf{r}, e)$ (movies in the Supplementary Information) show that $O_s^Q(\mathbf{r}, e)$ spatially fluctuates wildly in the entire energy range whereas the spatial fluctuation of $O_n^Q(\mathbf{r}, e)$ rapidly subsides as it approaches $e \approx 1$. This dramatic difference is summarized in plots of the correlation lengths $\xi_n(e)$ and $\xi_s(e)$ extracted from $O_n^Q(\mathbf{r}, e)$ and $O_s^Q(\mathbf{r}, e)$ (Fig. 4b), wherein $\xi_n(e)$ diverges to the FOV size at $e \approx 1$. The representative spatial images of $O_n^Q(\mathbf{r}, e=1)$ and $O_s^Q(\mathbf{r}, e=1)$ in Fig. 4c and d show how distinct are the spatial structures of $O_n^Q(\mathbf{r}, e)$ and $O_s^Q(\mathbf{r}, e)$.

Our results also provide a new perspective which, by using C_2 symmetry as a common theme, may help to unify the understanding of

Figure 3 | Nematic ordering and O-site specificity of

$\omega \approx \Delta_1$ pseudogap states. **a**, Topographic image $T(\mathbf{r})$ of the $\text{Bi}_2\text{Sr}_2\text{CaCu}_2\text{O}_{8+\delta}$ surface. The inset shows that the real part of its Fourier transform $\text{Re}T(\mathbf{q})$ does not break C_4 symmetry at its Bragg points because plots of $T(\mathbf{q})$ show its values to be indistinguishable at $\mathbf{Q}_x = (1, 0)2\pi/a_0$ and $\mathbf{Q}_y = (0, 1)2\pi/a_0$. Importantly, this means that neither the crystal nor the tip used to image it (and its $Z(\mathbf{r}, \omega)$ simultaneously) exhibits C_2 symmetry (Supplementary Information section V). The bulk incommensurate crystal supermodulation is seen clearly here; as always, it is at 45° to, and therefore is the mirror plane between, the x and y axes. For this symmetry reason it has no influence on the electronic nematicity discussed in this paper. **b**, The $Z(\mathbf{r}, e=1)$ image measured simultaneously with $T(\mathbf{r})$ in **a**. The inset shows that the Fourier transform $Z(\mathbf{q}, e=1)$ does break C_4 symmetry at its Bragg points because $\text{Re}\tilde{Z}(\mathbf{Q}_x, e=1) \neq \text{Re}\tilde{Z}(\mathbf{Q}_y, e=1)$. This means that, on average throughout the FOV of **a** and **b**, the modulations of $Z(\mathbf{r}, \omega \approx \Delta_1)$ that are periodic with the lattice have different intensities along the x axis and along the y axis. This is a priori evidence for electronic nematicity in the pseudogap states $\omega \approx \Delta_1$. **c**, The value of $O_n^Q(e)$ defined in equation (3) computed from $Z(\mathbf{r}, e)$ data measured in the same FOV as **a** and **b**. Its magnitude is low for all $\omega < \Delta_0$ and then rises rapidly to become well established near $e \approx 1$ or $\omega \approx \Delta_1$. Thus the quantitative measure of intra-unit-cell electronic nematicity established in equations (1) and (3) reveals that the pseudogap states in this FOV of a strongly underdoped $\text{Bi}_2\text{Sr}_2\text{CaCu}_2\text{O}_8$ sample are nematic. **d**, Topographic image $T(\mathbf{r})$ from the region identified by a small black box in **a**. It is labelled with the locations of the Cu atom plus both the O atoms within each CuO_2 unit cell (labels shown in the inset). Overlaid is the location and orientation of a Cu and four surrounding O atoms using a representation similar to that of Fig. 2c. **e**, The simultaneous $Z(\mathbf{r}, e=1)$ image in the same FOV as **d** (the region identified by small white box in **b**) showing the same Cu and O site labels within each unit cell (see inset). Thus the physical locations at which the nematic measure $O_n^R(e)$ of equation (4) is evaluated are labelled by the dashes. **f**, The value of $O_n^R(e)$ in equation (4) computed from $Z(\mathbf{r}, e)$ data measured in the same FOV as **a** and **b**. As in **c**, its magnitude is low for all $\omega < \Delta_0$ and then rises rapidly to become well established at $e \approx 1$ or $\omega \approx \Delta_1$. If the function in equation (4) is evaluated using the Cu sites only, the nematicity is about zero (black diamonds), as it must be. This independent quantitative measure of intra-unit-cell electronic nematicity $O_n^R(e)$ again shows that the pseudogap states are strongly nematic and, moreover, that the nematicity is due primarily to electronic inequivalence of the two O sites within each unit cell.

angle-resolved photoemission (ARPES), neutron scattering and spectroscopic-imaging STM studies of broken electronic symmetries within the pseudogap phase. ARPES reveals spontaneous dichroism of the $\mathbf{k} = (1, 0)\pi/a_0$ and $\mathbf{k} = (0, 1)\pi/a_0$ states²⁴, exhibiting C_2 symmetry because the opposite sign of the effect occurs at $\mathbf{k} = (1, 0)\pi/a_0$ and $\mathbf{k} = (0, 1)\pi/a_0$ (ref. 24). These excitations, which are probably magnetic, appear at T^* in $\text{Bi}_2\text{Sr}_2\text{CaCu}_2\text{O}_{8+\delta}$. The unusual magnetic order detected by polarized neutron diffraction at the Bragg peak^{25,26} consists of magnetic moments of about $0.1\mu_B$ (where μ_B is the Bohr magneton) exhibiting C_2 symmetry. These intra-unit-cell signals appear at T^* in both $\text{YBa}_2\text{Cu}_3\text{O}_{6+x}$ (ref. 25) and $\text{HgBa}_2\text{CuO}_{4+\delta}$ (ref. 26). Our studies reveal intra-unit-cell, C_2 symmetric excitations at the pseudogap energy and that these effects are associated primarily with electronic inequivalence at the two O sites within the CuO_2 unit cell. Given the many common characteristics observed by these diverse techniques, it is reasonable to consider whether ARPES, neutron diffraction and spectroscopic-imaging STM are detecting the same excitations with the same broken symmetries. If so, the pseudogap excitations of underdoped copper oxides would represent weakly magnetic states at the O sites within each CuO_2 unit cell, the electronic structure of which breaks C_4 symmetry. Then, the electronic symmetry breaking that occurs on entering the pseudogap phase would be due to the electronic nematic state visualized here, for the first time to our knowledge (Figs 3 and 4). Finally, the nematicity found in electronic transport²⁷, thermal transport²⁸ and the spin excitation spectrum²⁹ of $\text{YBa}_2\text{Cu}_3\text{O}_{6+x}$ could then occur because the Ising domains of $O_n^Q(\mathbf{r}, e)$ become aligned by the strong orthorhombicity of its crystal structure³⁰.

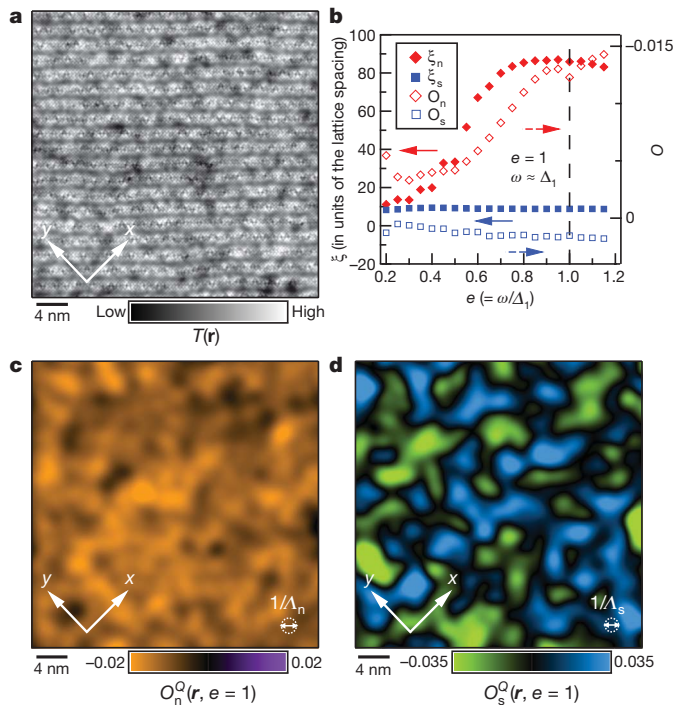


Figure 4 | Rapid increase of correlation length of nematicity at $\omega \approx \Delta_1$. **a**, A large FOV $T(\mathbf{r})$ image which preserves C_4 symmetry. **b**, Correlation lengths $\xi_n(e)$ for the nematic ordering $O_n^Q(\mathbf{r}, e)$ (red solid diamonds), and $\xi_s(e)$ for the possibly smectic ordering $O_s^Q(\mathbf{r}, e)$ (blue solid squares). (See Supplementary Information section VI for an evaluation of $O_n^Q(\mathbf{r}, e)$ and $O_s^Q(\mathbf{r}, e)$.) The coarsening length scales $1/\Lambda_n$ and $1/\Lambda_s$ are one-third that of typical spatial variations, as determined from the 3σ radius of the respective peaks. The correlation lengths are determined from the full-width at half-maximum of the spatial auto-correlation functions. Comparison of the nematic order parameter $O_n^Q(e)$ evaluated from equation (3) (open diamonds) and smectic order parameter $O_s^Q(e)$ from equation (6) (open squares) shows that $O_s^Q(e)$ has low magnitude and is energy independent, whereas $O_n^Q(e)$ rises rapidly to become well established at the pseudogap energy. **c**, Image of $O_n^Q(\mathbf{r}, e=1)$ (Supplementary Information section VI) from the same FOV showing that $\xi_n(e)$ has diverged to the size of the image. Thus, if there are Ising nematic domains (as there should be), they must be larger than 0.025 micrometres square. We note that the spatial resolution is limited by the cut-off scales shown in the figure. **d**, Images of $O_s^Q(\mathbf{r}, e=1)$ (Supplementary Information section VI) from the same FOV as a showing that $\xi_s(e)$ is spatially disordered with very short correlation length; this is equally true at all energies. The evolution of $O_n^Q(\mathbf{r}, e)$ and $O_s^Q(\mathbf{r}, e)$ as a function of e are available in Supplementary movies 1 and 2, respectively.

Received 5 March; accepted 4 May 2010.

- Orenstein, J. & Millis, A. J. Advances in the physics of high-temperature superconductivity. *Science* **288**, 468–474 (2000).
- Zaanen, J., Sawatzky, G. A. & Allen, J. W. Band gaps and electronic structure of transition-metal compounds. *Phys. Rev. Lett.* **55**, 418–421 (1985).
- Hüfner, S., Hossain, M. A., Damascelli, A. & Sawatzky, G. A. Two gaps make a high-temperature superconductor? *Rep. Prog. Phys.* **71**, 062501 (2008).
- Allredge, J. W. *et al.* Evolution of the electronic excitation spectrum with strongly diminishing hole density in superconducting $\text{Bi}_2\text{Sr}_2\text{CaCu}_2\text{O}_{8+\delta}$. *Nature Phys.* **4**, 319–326 (2008).
- Kohsaka, Y. *et al.* An intrinsic bond-centered electronic glass with unidirectional domains in underdoped cuprates. *Science* **315**, 1380–1385 (2007).
- Lee, J. *et al.* Spectroscopic fingerprint of phase-incoherent superconductivity in the cuprate pseudogap state. *Science* **325**, 1099–1103 (2009).
- McElroy, K. *et al.* Coincidence of checkerboard charge order and antinodal state decoherence in strongly underdoped superconducting $\text{Bi}_2\text{Sr}_2\text{CaCu}_2\text{O}_{8+\delta}$. *Phys. Rev. Lett.* **94**, 197005 (2005).
- Kohsaka, Y. *et al.* How Cooper pairs vanish approaching the Mott insulator in $\text{Bi}_2\text{Sr}_2\text{CaCu}_2\text{O}_{8+\delta}$. *Nature* **454**, 1072–1078 (2008).
- Maestro, A. D., Rosenow, B. & Sachdev, S. From stripe to checkerboard ordering of charge-density waves on the square lattice in the presence of quenched disorder. *Phys. Rev. B* **74**, 024520 (2006).

- Robertson, J. A., Kivelson, S. A., Fradkin, E., Fang, A. C. & Kapitulnik, A. Distinguishing patterns of charge order: stripes or checkerboards. *Phys. Rev. B* **74**, 134507 (2006).
- Kivelson, S. A., Fradkin, E. & Emery, V. J. Electronic liquid-crystal phases of a doped Mott insulator. *Nature* **393**, 550–553 (1998).
- Kivelson, S. A. *et al.* How to detect fluctuating stripes in the high-temperature superconductors. *Rev. Mod. Phys.* **75**, 1201–1241 (2003).
- Sachdev, S. Colloquium: order and quantum phase transitions in the cuprate superconductors. *Rev. Mod. Phys.* **75**, 913–932 (2003).
- Vojta, M. Lattice symmetry breaking in cuprate superconductors: stripes, nematics, and superconductivity. *Adv. Phys.* **58**, 699–820 (2009).
- Kim, E.-A. *et al.* Theory of the nodal nematic quantum phase transition in superconductors. *Phys. Rev. B* **77**, 184514 (2008).
- Fradkin, E., Kivelson, S. A., Lawler, M. J., Eisenstein, J. P. & Mackenzie, A. P. Nematic Fermi fluids in condensed matter physics. *Annu. Rev. Condens. Matter Phys.* **1**, 7.1–7.26 (2010).
- Cvetkovic, V., Nussinov, Z., Mukhin, S. & Zaanen, J. Observing the fluctuating stripes in high- T_c superconductors. *Europhys. Lett.* **81**, 27001 (2008).
- Borzi, R. A. *et al.* Formation of a nematic fluid at high fields in $\text{Sr}_3\text{Ru}_2\text{O}_7$. *Science* **315**, 214–217 (2007).
- Chuang, T.-M. *et al.* Nematic electronic structure in the “parent” state of the iron-based superconductor $\text{Ca}(\text{Fe}_{1-x}\text{Co}_x)_2\text{As}_2$. *Science* **327**, 181–184 (2010).
- Raghu, S. *et al.* Microscopic theory of the nematic phase in $\text{Sr}_3\text{Ru}_2\text{O}_7$. *Phys. Rev. B* **79**, 214402 (2009).
- Lv, W. Wu, J. & Phillips, P. Orbital ordering induces structural phase transition and the resistivity anomaly in iron pnictides. *Phys. Rev. B* **80**, 224506 (2009).
- Lee, W.-C. & Wu, C. Theory of unconventional metamagnetic electron states in orbital band systems. *Phys. Rev. B* **80**, 104438 (2009).
- Krüger, F., Kumar, S., Zaanen, J. & van den Brink, J. Spin-orbital frustrations and anomalous metallic state in iron-pnictide superconductors. *Phys. Rev. B* **79**, 054504 (2009).
- Kaminski, A. *et al.* Spontaneous breaking of time-reversal symmetry in the pseudogap state of a high- T_c superconductor. *Nature* **416**, 610–613 (2002).
- Fauqué, B. *et al.* Magnetic order in the pseudogap phase of high- T_c superconductors. *Phys. Rev. Lett.* **96**, 197001 (2006).
- Li, Y. *et al.* Unusual magnetic order in the pseudogap region of the superconductor $\text{HgBa}_2\text{CuO}_{4+\delta}$. *Nature* **455**, 372–375 (2008).
- Sun, X. F., Segawa, K. & Ando, Y. Metal-to-insulator crossover in $\text{YBa}_2\text{Cu}_3\text{O}_y$ probed by low-temperature quasiparticle heat transport. *Phys. Rev. Lett.* **93**, 107001 (2004).
- Daou, R. *et al.* Broken rotational symmetry in the pseudogap phase of a high- T_c superconductor. *Nature* **463**, 519–522 (2010).
- Hinkov, V. *et al.* Electronic liquid crystal state in the high-temperature superconductor $\text{YBa}_2\text{Cu}_3\text{O}_{6.45}$. *Science* **319**, 597–600 (2008).
- Sun, K., Lawler, M. J. & Kim, E.-A. Spin-charge interplay in electronic liquid crystals: fluctuating spin stripe driven by charge nematic. *Phys. Rev. Lett.* **104**, 106405 (2010).

Supplementary Information is linked to the online version of the paper at www.nature.com/nature.

Acknowledgements We are grateful to P. Abbamonte, D. Bonn, J.C. Campuzano, D.M. Egler, E. Fradkin, T. Hanaguri, W. Hardy, J. E. Hoffman, S. Kivelson, A.P. Mackenzie, M. Norman, B. Ramshaw, S. Sachdev, G. Sawatzky, H. Takagi, J. Tranquada and J. Zaanen, for discussions and communications. Theoretical studies were supported by NSF DMR-0520404 to the Cornell Center for Materials Research. Experimental studies are supported by the Center for Emergent Superconductivity, an Energy Frontier Research Center, headquartered at Brookhaven National Laboratory and funded by the US Department of Energy, under DE-2009-BNL-PM015, as well as by a Grant-in-Aid for Scientific Research from the Ministry of Science and Education (Japan) and the Global Centers of Excellence Program for Japan Society for the Promotion of Science. A.R.S. acknowledges support from the US Army Research Office. M.J.L., J.C.D. and E.-A.K. thank KITP for its hospitality. J.C.D. acknowledges gratefully the hospitality and support of the Physics and Astronomy Department at the University of British Columbia, Vancouver, Canada.

Author Contributions M.J.L. and E.-A.K. led the theoretical studies and initially observed the possibility of nematic order in electronic structure images; M.J.L., K.F. and J.P.S. developed the data analysis algorithms and carried out the analysis; K.F., J.L., C.K.K., A.R.S. and Y.K. carried out the experiments and systematic tests; K.F., H.E. and S.U. synthesized the sequence of samples; K.F. was responsible for the figures and SOM; E.-A.K., J.C.D. and M.J.L. supervised the investigation and wrote the paper. The manuscript reflects the contributions of all authors.

Author Information Reprints and permissions information is available at www.nature.com/reprints. The authors declare no competing financial interests. Readers are welcome to comment on the online version of this article at www.nature.com/nature. Correspondence and requests for materials should be addressed to E.-A.K. (euon-ah.kim@cornell.edu).